

A collocation method for nonlinear tensor differential equations on low-rank manifolds

Alec Dektor^{a,*}

^a*Applied Mathematics & Computational Research Division, Lawrence Berkeley National Laboratory, Berkeley (CA) 94720, USA.*

Abstract

We present a new method to compute the solution to a nonlinear tensor differential equation with dynamical low-rank approximation. The idea of dynamical low-rank approximation is to project the differential equation onto the tangent space of a low-rank tensor manifold at each time. Traditionally, an orthogonal projection onto the tangent space is employed, which is challenging to compute for nonlinear differential equations. We introduce a novel interpolatory projection onto the tangent space that is easily computed for many nonlinear differential equations and satisfies the differential equation at a set of carefully selected indices. To select these indices, we devise a new algorithm based on the discrete empirical interpolation method (DEIM) that parameterizes any tensor train and its tangent space with tensor cross interpolants. We demonstrate the proposed method with applications to tensor differential equations arising from the discretization of partial differential equations.

1. Introduction

Consider the initial value problem

$$\frac{\partial u(\mathbf{x}, t)}{\partial t} = \mathcal{G}(u, \mathbf{x}, t), \quad u(\mathbf{x}, 0) = u_0(\mathbf{x}), \quad (1)$$

governing the time evolution of a quantity of interest $u : \Omega \times [0, T] \rightarrow \mathbb{R}$, where Ω is a subset of \mathbb{R}^d ($d \gg 1$) and \mathcal{G} is a nonlinear operator that may depend on \mathbf{x} and t . Equations of the form (1) are found in many areas of physical sciences, engineering, and mathematics. For example, in applications of kinetic theory such as the Fokker–Planck equation [27] and the Boltzmann equation [2], in optimal mass transport [14], and as finite-dimensional approximations of functional differential equations [33, 32]. Discretizing (1) with a method of lines yields the tensor differential equation

$$\frac{d\mathbf{u}(t)}{dt} = G(\mathbf{u}, t), \quad \mathbf{u}(0) = \mathbf{u}_0, \quad (2)$$

where $\mathbf{u}(t) : [0, T] \rightarrow \mathbb{R}^{n_1 \times \dots \times n_d}$ is the time-dependent solution tensor and $G : \mathbb{R}^{n_1 \times \dots \times n_d} \times [0, T] \rightarrow \mathbb{R}^{n_1 \times \dots \times n_d}$ is the discrete form of the operator \mathcal{G} corresponding to the discretization scheme. At any time t , the solution tensor $\mathbf{u}(t)$ has $\mathcal{O}(n^d)$ degrees of freedom that make its computation and storage prohibitively expensive, even for small d .

Recently, significant research efforts have been made [3, 21, 8, 9, 4, 28, 19, 11, 10, 7] to develop methods that reduce the computational and storage costs of solving (2) by integrating an approximate solution $\mathbf{f}(t)$ on a low-rank tensor manifold $\mathcal{M} \subset \mathbb{R}^{n_1 \times \dots \times n_d}$. The manifold \mathcal{M} is defined by a low-rank tensor format and a tensor rank r , which are chosen so that the tensors in \mathcal{M} can be parameterized with significantly fewer degrees of freedom than $\mathcal{O}(n^d)$. For example, using the tensor train (TT) format, the manifold \mathcal{M} contains tensors that can be parameterized with $\mathcal{O}(dnr^2)$ degrees of freedom, a significant reduction when r is relatively small. A fundamental concept for performing time integration on \mathcal{M} is dynamical low-rank approximation. The idea is to integrate $\mathbf{f}(t)$ on \mathcal{M} by identifying a tensor $d\mathbf{f}(t)/dt$ that is tangent to \mathcal{M} at each time t . When computing an approximate solution $\mathbf{f}(t)$ to (2), the tangent tensor $d\mathbf{f}(t)/dt$ is chosen as an approximation to $G(\mathbf{f}, t)$. In other words, dynamical low-rank methods for approximating (2) on \mathcal{M} minimize the residual

$$\mathbf{R}_{\mathcal{M}}(t) = \frac{d\mathbf{f}(t)}{dt} - G(\mathbf{f}, t), \quad (3)$$

*Corresponding author

Email address: adektor@lbl.gov (Alec Dektor)

over tensors $d\mathbf{f}(t)/dt$ in the tangent space $T_{\mathbf{f}(t)}\mathcal{M}$ at each time t . In order to obtain a practical method for integrating $\mathbf{f}(t)$ on \mathcal{M} , it is crucial to compute $d\mathbf{f}(t)/dt$ at a reasonable computational cost at each time t . Traditional dynamical low-rank methods minimize the Frobenius norm of the residual (3), which uniquely identifies $d\mathbf{f}(t)/dt$ as the orthogonal projection of $G(\mathbf{f}, t)$ onto the tangent space $T_{\mathbf{f}(t)}\mathcal{M}$ (see, e.g., [21]). Computing such orthogonal projection at a reasonable cost requires obtaining $G(\mathbf{f}, t)$ as a low-rank tensor, which can be challenging, especially when G is nonlinear. For example, when G includes a polynomial nonlinearity, computing $G(\mathbf{f}, t)$ as a low-rank tensor can be expensive due to the non-optimal tensor rank that results from multiplying low-rank tensors. The situation can be worse for other common nonlinearities, such as exponential or fractional, as dependable algorithms for performing these nonlinear arithmetic operations with low-rank tensors do not exist.

In this paper we propose a new time integration method for (2) on the low-rank tensor manifold \mathcal{M} that does not require computing $G(\mathbf{f}, t)$ in a low-rank format and is computationally efficient for nonlinear G . Instead of minimizing the norm of the residual (3), we select a tangent tensor $d\mathbf{f}(t)/dt$ so that the residual (3) vanishes at a set of carefully chosen indices $\{\mathcal{I}^{\leq k}, \mathcal{I}^{> k}\}$

$$\mathbf{R}_{\mathcal{M}}(t; \mathcal{I}^{\leq k-1}, i_k, \mathcal{I}^{> k}) = 0, \quad k = 1, 2, \dots, d, \quad (4)$$

at each time t . To select these indices, we devise a new algorithm based on the discrete empirical interpolation method (DEIM) that parameterizes any tensor train (TT) with a tensor cross interpolant. This index selection algorithm, referred to as TT-cross-DEIM, extends the DEIM induced matrix CUR factorization introduced in [30] to tensors in the TT format. Using the indices determined by TT-cross-DEIM, we show that there exists a unique tensor tangent to \mathcal{M} at each time t satisfying (4). This tangent tensor allows us to integrate $\mathbf{f}(t)$ on \mathcal{M} by evaluating the tensor $G(\mathbf{f}, t)$ at a small subset of indices, which is efficient to compute when G is nonlinear. Related time integration schemes have recently been proposed in [13, 22] for computing a low-rank approximation to matrix differential equations.

The rest of this paper is organized as follows. In Section 2, we recall the TT format and tensor cross approximation and present the TT-cross-DEIM index selection algorithm. We show that the TT-cross-DEIM determines indices that parameterize any TT with a tensor cross interpolant. In Section 3, we parameterize the tangent space of \mathcal{M} with interpolants using the TT-cross-DEIM indices and propose a new dynamical low-rank time integration scheme that is efficient for nonlinear tensor differential equations (2). In Section 4, we demonstrate the proposed dynamical low-rank collocation method and compare the results with existing time integration methods on low-rank tensor manifolds. The main findings are summarized in Section 5.

2. Tensor train format and cross interpolation

Any tensor $\mathbf{f} \in \mathbb{R}^{n_1 \times \dots \times n_d}$ can be represented in the tensor train (TT) format as

$$\mathbf{f}(i_1, i_2, \dots, i_d) = \mathbf{C}_1(i_1)\mathbf{C}_2(i_2) \cdots \mathbf{C}_d(i_d), \quad (5)$$

where each \mathbf{C}_k is a $r_{k-1} \times n_k \times r_k$ tensor (with $r_0 = r_d = 1$), referred to as a TT-core. The TT format parameterizes \mathbf{f} using d TT-cores with a total of $\sum_{i=1}^d r_{i-1}r_i n_i$ degrees of freedom. This number can be significantly smaller than the $n_1 n_2 \cdots n_d$ degrees of freedom in \mathbf{f} , especially as the dimension d grows, provided the ranks r_i are small. We denote by $\mathbf{C}_k^{(l)} \in \mathbb{R}^{r_{k-1} n_k \times r_k}$ and $\mathbf{C}_k^{(r)} \in \mathbb{R}^{r_{k-1} \times n_k r_k}$ the left and right unfolding matrices obtained from reshaping the elements of \mathbf{C}_k so that

$$\mathbf{C}_k^{(l)}(\alpha_{k-1} i_k, \alpha_k) = \mathbf{C}_k^{(r)}(\alpha_{k-1}, i_k \alpha_k) = \mathbf{C}_k(\alpha_{k-1}, i_k, \alpha_k), \quad k = 1, 2, \dots, d.$$

The tensor \mathbf{f} has TT-rank (or rank if TT is clear from context) $\mathbf{r} = (r_0, r_1, \dots, r_d)$ if the unfolding matrices $\mathbf{C}_k^{(l)}$ and $\mathbf{C}_k^{(r)}$ have full rank for all $k = 1, 2, \dots, d$. A specific instance of the TT format (5) is a generalization of matrix CUR decomposition to tensors, referred to as tensor cross approximation, wherein the cores are defined in terms of the entries of \mathbf{f} [12, 23, 29, 26]

$$\tilde{\mathbf{f}}(i_1, \dots, i_d) = \prod_{k=1}^d \mathbf{f}(\mathcal{I}^{\leq k-1}, i_k, \mathcal{I}^{> k}) [\mathbf{f}(\mathcal{I}^{\leq k}, \mathcal{I}^{> k})]^\dagger. \quad (6)$$

Here, $\mathcal{I}^{\leq k}$ is a subset of indices from $\mathbb{I}_{n_1} \times \dots \times \mathbb{I}_{n_k}$ and $\mathcal{I}^{> k}$ is a subset of indices from $\mathbb{I}_{n_{k+1}} \times \dots \times \mathbb{I}_{n_d}$ where $\mathbb{I}_{n_j} = \{1, 2, \dots, n_j\}$, and \dagger denotes the Moore–Penrose pseudoinverse. We assume that $\mathcal{I}^{\leq k}$ and $\mathcal{I}^{> k}$ have the same

cardinality for all $k = 1, 2, \dots, d-1$ and for convenience set $\mathcal{I}^{\leq 0} = \mathcal{I}^{> d} = \emptyset$. Several algorithms for computing tensor cross approximations (6) from blackbox tensors \mathbf{f} based on the maximum volume principle have recently been developed [23, 12]. Hereafter we present a new method for computing tensor cross approximations (6) from a given TT representation (5) based on the DEIM index selection algorithm.

2.1. Tensor train cross DEIM

The DEIM index selection algorithm was initially introduced in [5] for model order reduction in nonlinear vector differential equations. Subsequently, the algorithm was applied to obtain matrix cross (also known as CUR) approximations from the singular vectors of the matrix [30] and more recently, to obtain tensor cross approximations in the Tucker format [15]. We now devise a new algorithm to obtain a TT-cross approximation (6) from a rank- r TT (5) using the DEIM. The proposed algorithm, which we refer to as the TT-cross discrete empirical interpolation method (TT-cross-DEIM), applies the DEIM index selection algorithm to singular vectors in each of the SVDs

$$\mathbf{f}^{(k)} = \mathbf{W}_{\leq k} \mathbf{\Sigma}_k \mathbf{V}_{> k}^T, \quad k = 1, 2, \dots, d-1. \quad (7)$$

Here, $\mathbf{f}^{(k)} \in \mathbb{R}^{(n_1 \cdots n_k) \times (n_{k+1} \cdots n_d)}$ denotes the k th unfolding matrix obtained from reshaping the elements of \mathbf{f} so that $\mathbf{f}^{(k)}(i_1 \cdots i_k, i_{k+1} \cdots i_d) = \mathbf{f}(i_1, \dots, i_d)$, which is a rank- r_k matrix if \mathbf{f} is a rank- r TT. When $d = 2$, there is only one unfolding matrix in (7) and the proposed TT-cross-DEIM algorithm is equivalent to the DEIM induced matrix cross approximation introduced in [30]. In this case, the DEIM index selection algorithm is applied to $\mathbf{W}_{\leq 1}$ and $\mathbf{V}_{> 1}$ to obtain $s_1 \leq r_1$ row indices $\mathcal{I}^{\leq 1}$ and s_1 column indices $\mathcal{I}^{> 1}$ so that the resulting rank- s_1 matrix cross approximation

$$\mathbf{f}(i_1, i_2) \approx \mathbf{f}(i_1, \mathcal{I}^{> 1}) [\mathbf{f}(\mathcal{I}^{\leq 1}, \mathcal{I}^{> 1})]^{-1} \mathbf{f}(\mathcal{I}^{\leq 1}, i_2),$$

is nearly as accurate as the rank- s_1 truncated SVD of \mathbf{f} .

When $d > 2$, the left and right singular vector matrices $\mathbf{W}_{\leq k}$ and $\mathbf{V}_{> k}$ in (7) have dimensions $(n_1 \cdots n_k) \times r_k$ and $(n_{k+1} \cdots n_d) \times r_k$, respectively. To avoid constructing these large singular vector matrices explicitly, we access them via the TT-SVD representation. Recall that given a TT representation (5), the TT-SVD representation

$$\mathbf{f}(i_1, \dots, i_d) = \mathbf{W}_1(i_1) \cdots \mathbf{W}_k(i_k) \mathbf{\Sigma}_k \mathbf{V}_{k+1}(i_{k+1}) \cdots \mathbf{V}_d(i_d), \quad (8)$$

can be computed by executing a sequence of QR-decompositions on unfoldings of TT-cores followed by a SVD of a $r_k \times r_k$ matrix [24]. In (8), the cores \mathbf{W}_j are left-orthogonal, the cores \mathbf{V}_j are right-orthogonal, i.e.,

$$\begin{aligned} \left(\mathbf{W}_j^{(l)} \right)^T \mathbf{W}_j^{(l)} &= \mathbf{I}_{r_j \times r_j}, & j = 1, \dots, k, \\ \mathbf{V}_j^{(r)} \left(\mathbf{V}_j^{(r)} \right)^T &= \mathbf{I}_{r_{j-1} \times r_{j-1}}, & j = k+1, \dots, d, \end{aligned} \quad (9)$$

and $\mathbf{\Sigma}_k$ is the $r_k \times r_k$ diagonal matrix of singular values in (7). The left singular vectors in (7) can be expressed as a product of the left-orthogonal cores, and similarly, the right singular vectors as a product of the right-orthogonal cores

$$\begin{aligned} \mathbf{W}_{\leq k}(i_1 \cdots i_k, \alpha_k) &= \mathbf{W}_1(i_1) \cdots \mathbf{W}_k(i_k, \alpha_k), \\ \mathbf{V}_{> k}(i_{k+1} \cdots i_d, \alpha_k) &= \mathbf{V}_{k+1}(\alpha_k, i_{k+1}) \cdots \mathbf{V}_d(i_d). \end{aligned} \quad (10)$$

To avoid applying the DEIM algorithm to the large singular vector matrices (10), we compute collections of s_k indices $\mathcal{I}^{\leq k}$ sequentially for $k = 1, 2, \dots, d-1$ as follows. After computing s_{k-1} indices $\mathcal{I}^{\leq k-1}$, we obtain s_k indices $\mathcal{I}^{\leq k}$ by applying the DEIM algorithm to the $(s_{k-1} n_k) \times r_k$ matrix $\widehat{\mathbf{W}}_{\leq k}$ obtained from restricting $\mathbf{W}_{\leq k}$ to the s_{k-1} indices $\mathcal{I}^{\leq k-1}$. Likewise, the collections of s_k indices $\mathcal{I}^{> k}$ are computed sequentially for $k = d-1, d-2, \dots, 1$ by applying the DEIM algorithm to the $(s_{k+1} n_{k+1}) \times r_k$ matrix $\widehat{\mathbf{V}}_{> k}$ obtained from restricting $\mathbf{V}_{> k}$ to the s_{k+1} indices $\mathcal{I}^{> k+1}$.

2.1.1. The TT-cross-DEIM algorithm

We now present the TT-cross-DEIM algorithm for computing index sets $\{\mathcal{I}^{\leq j}, \mathcal{I}^{> j}\}$ defining a rank- s tensor cross approximation (6) from the TT representation (5) of the rank- r tensor \mathbf{f} . We assume that $s_k \leq r_k$ for all $k = 1, 2, \dots, d-1$ and denote by $\text{DEIM}_s(\cdot)$ a subroutine that takes a matrix of size $m \times r$ as input and outputs a collection of $s \leq r$ indices computed with the DEIM index selection algorithm (see, e.g., [30, Algorithm 1]). We first

describe the computation of indices $\mathcal{I}^{\leq j}$ for $j = 1, 2, \dots, d-1$ and subsequently describe the computation of $\mathcal{I}^{> j}$ for $j = d-1, d-2, \dots, 1$.

To begin, we use the TT-SVD algorithm [24, Section 3] to express \mathbf{f} in the form (8) with $k = 1$. From the TT-core \mathbf{W}_1 , which contains the left singular vectors of $\mathbf{f}^{(1)}$ (see (10)), we obtain s_1 indices

$$\mathcal{I}^{\leq 1} = \text{DEIM}_{s_1} \left(\mathbf{W}_1^{(l)} \right). \quad (11)$$

Next we obtain the TT-SVD representation (8) with $k = 2$ by taking a SVD of the $r_1 n_2 \times r_2$ matrix

$$(\boldsymbol{\Sigma}_1 \mathbf{V}_2)^{(l)} = \mathbf{W}_2^{(l)} \boldsymbol{\Sigma}_2 \mathbf{K}_2^T, \quad (12)$$

and redefining $\mathbf{V}_2 = \mathbf{K}_2^T \mathbf{V}_2$. Then we construct the $s_1 n_2 \times r_2$ matrix

$$\widehat{\mathbf{W}}_{\leq 2}(\beta_1 i_2, \alpha_2) = \sum_{\alpha_1=1}^{r_1} \mathbf{W}_1 \left(\mathcal{I}_{\beta_1}^{\leq 1}, \alpha_1 \right) \mathbf{W}_2(\alpha_1, i_2, \alpha_2), \quad (13)$$

where $\mathcal{I}_{\beta_1}^{\leq 1}$ denotes the β_1 st index in the collection $\mathcal{I}^{\leq 1}$. In light of (10), (13) is the restriction of the left singular vector matrix $\mathbf{W}_{\leq 2}$ of $\mathbf{f}^{(2)}$ to the indices $\mathcal{I}^{\leq 1}$. Applying the DEIM to $\widehat{\mathbf{W}}_2$ yields s_2 indices

$$\mathbf{l}_{\leq 2} = \text{DEIM}_{s_2} \left(\widehat{\mathbf{W}}_2 \right), \quad (14)$$

which we reshape into multi-indices $(\mathbf{p}_{<2}(\beta_2), \mathcal{I}_2(\beta_2))_{\beta_2=1}^{r_2}$, e.g., with a call to MATLAB's `ind2sub` function, so that $\mathbf{p}_{<2}(\beta_2)$ identifies an index in $\mathcal{I}^{\leq 1}$ and $\mathcal{I}_2(\beta_2)$ identifies an index in \mathbb{I}_{n_2} . From these multi-indices, we construct the tensor cross index set $\mathcal{I}^{\leq 2}$

$$\mathcal{I}_{\beta_2}^{\leq 2} = \left(\mathcal{I}_{\mathbf{p}_{<2}(\beta_2)}^{\leq 1}, \mathcal{I}_2(\beta_2) \right), \quad \beta_2 = 1, 2, \dots, s_2. \quad (15)$$

This process is repeated recursively as follows. After computing $\mathcal{I}^{\leq j-1}$ from the TT-SVD representation (8) with $k = j-1$, we obtain the cores in the $k = j$ TT-SVD representation of \mathbf{f} by taking a SVD of the $r_{j-1} n_j \times r_j$ matrix

$$(\boldsymbol{\Sigma}_{j-1} \mathbf{V}_j)^{(l)} = \mathbf{W}_j^{(l)} \boldsymbol{\Sigma}_j \mathbf{K}_{j+1}^T, \quad (16)$$

and redefining

$$\mathbf{V}_{j+1} = \mathbf{K}_{j+1}^T \mathbf{V}_{j+1}. \quad (17)$$

Then we construct the $s_{j-1} n_j \times r_j$ matrix $\widehat{\mathbf{W}}_{\leq j}$ by restricting $\mathbf{W}_{\leq j}$ to the indices $\mathcal{I}^{\leq j-1}$ using the expression (10) for $\mathbf{W}_{\leq j}$ in terms of left-orthogonal TT-cores

$$\begin{aligned} \widehat{\mathbf{W}}_{\leq j}(\beta_{j-1} i_j, \alpha_j) &= \sum_{\alpha_1=1}^{r_1} \cdots \sum_{\alpha_{j-1}=1}^{r_{j-1}} \mathbf{W}_1 \left(1, \mathcal{I}_{\beta_{j-1}}^{\leq j-1}(1), \alpha_1 \right) \cdots \\ &\quad \times \mathbf{W}_{j-1} \left(\alpha_{j-2}, \mathcal{I}_{\beta_{j-1}}^{\leq j-1}(j-1), \alpha_{j-1} \right) \mathbf{W}_j(\alpha_{j-1}, i_j, \alpha_j), \end{aligned} \quad (18)$$

where $\mathcal{I}_{\beta_{j-1}}^{\leq j-1}(i)$ denotes index i in the β_{j-1} st multi-index of $\mathcal{I}^{\leq j-1}$. Applying the DEIM algorithm to $\widehat{\mathbf{W}}_j$ yields s_j indices

$$\mathbf{l}_{\leq j} = \text{DEIM}_{s_j} \left(\widehat{\mathbf{W}}_j \right), \quad (19)$$

from which we obtain multi-indices $(\mathbf{p}_{<j}(\beta_j), \mathcal{I}_j(\beta_j))_{\beta_j=1}^{s_j}$ where $\mathbf{p}_{<j}(\beta_j)$ identifies an index in $\mathcal{I}^{\leq j-1}$ and $\mathcal{I}_j(\beta_j)$ identifies an index in \mathbb{I}_{n_j} . We then construct the tensor cross indices

$$\mathcal{I}_{\beta_j}^{\leq j} = \left(\mathcal{I}_{\mathbf{p}_{<j}(\beta_j)}^{\leq j-1}, \mathcal{I}_j(\beta_j) \right), \quad \beta_j = 1, 2, \dots, s_j. \quad (20)$$

This process is repeated for $j = 2, 3, \dots, d-1$ to obtain the tensor cross indices $\mathcal{I}^{\leq j}$.

The tensor cross indices $\mathcal{I}^{>j}$ for $j = d-1, d-2, \dots, 1$ are constructed with a similar procedure, beginning with the $k = d-1$ TT-SVD representation (8). From the TT-core \mathbf{V}_d , which contains the right singular vectors of $\mathbf{f}^{(d-1)}$ (see (10)), we obtain s_{d-1} indices

$$\mathcal{I}^{>d-1} = \text{DEIM}_{r_{d-1}} \left(\left[\mathbf{V}_d^{(r)} \right]^T \right). \quad (21)$$

The remainder of the tensor cross indices $\mathcal{I}^{>j}$ for $j = d-2, d-3, \dots, 1$ are obtained recursively as follows. After computing $\mathcal{I}^{>j+1}$ from the TT-SVD representation (8) with $k = j+1$, we obtain the cores in the $k = j$ TT-SVD (8) by taking a SVD of the $r_j \times n_{j+1} r_{j+1}$ matrix

$$(\mathbf{W}_{j+1} \boldsymbol{\Sigma}_{j+1})^{(r)} = \mathbf{U}_j \boldsymbol{\Sigma}_j \mathbf{V}_{j+1}^{(r)}, \quad (22)$$

and redefining

$$\mathbf{W}_j = \mathbf{W}_j \mathbf{U}_j. \quad (23)$$

Then we construct the $s_{j+1} n_j \times r_j$ matrix $\widehat{\mathbf{V}}_{>j}$ by restricting $\mathbf{V}_{>j}$ to the indices $\mathcal{I}^{>j+1}$ using the expression (10) for $\mathbf{V}_{>j}$ in terms of right-orthogonal TT-cores

$$\begin{aligned} \widehat{\mathbf{V}}_{>j}(i_{j+1} \beta_{j+1}, \alpha_j) &= \sum_{\alpha_{j+1}=1}^{r_{j+1}} \cdots \sum_{\alpha_{d-1}=1}^{r_{d-1}} \mathbf{V}_{j+1}(\alpha_j, i_{j+1}, \alpha_{j+1}) \\ &\times \mathbf{V}_{j+2}(\alpha_{j+1}, \mathcal{I}_{\beta_{j+1}}^{>j+1}(j+2), \alpha_{j+2}) \cdots \mathbf{V}_d(\alpha_{d-1}, \mathcal{I}_{\beta_{j+1}}^{>j+1}(d), 1), \end{aligned} \quad (24)$$

where $\mathcal{I}_{\beta_{j+1}}^{>j+1}(i)$ denotes the index corresponding to dimension i in the β_{j+1} multi-index of $\mathcal{I}^{>j+1}$. Applying the DEIM algorithm to $\widehat{\mathbf{V}}_{>j}$ yields s_j indices

$$\mathbf{l}_{>j} = \text{DEIM}_{s_j} \left(\widehat{\mathbf{V}}_{>j} \right), \quad (25)$$

from which we obtain multi-indices $(\mathcal{J}_{j+1}(\beta_j), \mathbf{p}_{>j+1}(\beta_j))_{\beta_j=1}^{s_j}$, where $\mathcal{J}_{j+1}(\beta_j)$ corresponds to a index from $\mathbb{I}_{n_{j+1}}$ while $\mathbf{p}_{>j+1}(\beta_j)$ corresponds to a multi-index from the set $\mathcal{I}^{>j+1}$. We then construct the tensor cross indices

$$\mathcal{I}_{\beta_j}^{>j} = \left(\mathcal{J}_{j+1}(\beta_j), \mathcal{I}_{\mathbf{p}_{>j+1}(\beta_j)}^{>j+1} \right), \quad \beta_j = 1, 2, \dots, s_j. \quad (26)$$

This process is repeated for $j = d-2, d-3, \dots, 1$ to obtain the tensor cross indices $\mathcal{I}^{>j}$.

The TT-cross-DEIM algorithm for computing tensor cross indices $\{\mathcal{I}^{\leq j}, \mathcal{I}^{>j}\}$ from the TT representation (5) is summarized in Algorithm 1. During the computation of $\mathcal{I}^{>j}$ for $j = 1, 2, \dots, d-1$ all $d-1$ TT-SVD representations (8) required for the computation of $\mathcal{I}^{>j}$ are computed. Therefore, one may store these orthogonal cores during the computation of $\mathcal{I}^{\leq j}$ and reuse them for the computation of $\mathcal{I}^{>j}$ instead of recomputing them, as described in (22)-(23). Finally, we point out that the TT-SVD truncation algorithm also requires the $d-1$ TT-SVD representations (5). Therefore we can combine the TT-SVD truncation and TT-cross-DEIM algorithms to simultaneously truncate a TT and compute tensor cross index sets.

Computational cost. To simplify the floating point operation count of the proposed TT-cross-DEIM (Algorithm 1), we assume that $r_k = s_k = r$ and $n_k = n$ for all $k = 1, 2, \dots, d$. The Algorithm requires access to all $d-1$ orthogonal representations (8) which can be computed in $\mathcal{O}(dnr^3)$ FLOPS [24]. With these orthogonal representations available, each multi-index set $\mathcal{I}^{\leq k}$ and $\mathcal{I}^{>k}$ for $k = 1, 2, \dots, d-1$ is computed by applying DEIM to a matrix of size $rn \times r$ each of which requires $\mathcal{O}(nr)$ operations. Therefore the total estimate for the number of FLOPS in the TT-cross-DEIM Algorithm 1 is $\mathcal{O}(dnr^3)$.

2.2. Accuracy of the TT-cross-DEIM

Notice that $\mathcal{I}^{\leq k}, \mathcal{I}^{>k}$ obtained with the TT-cross-DEIM Algorithm in (20), (26) satisfy

$$\mathcal{I}^{\leq k} \subset \mathcal{I}^{\leq k-1} \times \mathbb{I}_k, \quad \mathcal{I}^{>k} \subset \mathbb{I}_k \times \mathcal{I}^{>k+1}, \quad k = 1, 2, \dots, d-1, \quad (27)$$

by construction. The condition (27) is sufficient for the tensor cross approximation (6) to interpolate (5) at $\mathcal{I}^{\leq k}, \mathcal{I}^{>k}$ [12]

$$\tilde{\mathbf{f}}(\mathcal{I}^{\leq k-1}, :, \mathcal{I}^{>k}) = \mathbf{f}(\mathcal{I}^{\leq k-1}, :, \mathcal{I}^{>k}), \quad k = 1, 2, \dots, d, \quad (28)$$

Algorithm 1 TT-cross discrete empirical interpolation method (TT-cross-DEIM) algorithm.

Require:

C_1, C_2, \dots, C_d , TT-cores of rank- r tensor f
 s , desired TT-rank of tensor cross interpolant

Ensure:

$\{\mathcal{I}^{\leq j}, \mathcal{I}^{> j}\}$, nested index sets for TT-cross approximation (6)

- 1: $\mathbf{f} = \mathbf{W}_1 \boldsymbol{\Sigma}_1 \mathbf{V}_2 \cdots \mathbf{V}_d$ ▷ TT-SVD (8) with $k = 1$
 - 2: $\mathcal{I}^{\leq 1} = \text{DEIM}_{s_1}(\mathbf{W}_1^{(l)})$
 - 3: **for** $j = 2$ **to** $d - 1$ **do**
 - 4: $(\boldsymbol{\Sigma}_{j-1} \mathbf{V}_j)^{(l)} = \mathbf{W}_j^{(l)} \boldsymbol{\Sigma}_j \mathbf{K}_{j+1}^T$
 - 5: $\mathbf{V}_{j+1} = \mathbf{K}_{j+1}^T \mathbf{V}_{j+1}$ ▷ TT-SVD (8) with $k = j$
 - 6: $\widehat{\mathbf{W}}_{\leq j}(\beta_{j-1} i_j, \alpha_j) = \mathbf{W}_{\leq j}(\mathcal{I}_{\beta_{j-1}}^{\leq j-1} i_j, \alpha_j)$ ▷ restrict left singular vectors
 - 7: $\mathbf{l}_{\leq j} = \text{DEIM}_{s_j}(\widehat{\mathbf{W}}_j)$
 - 8: $\mathbf{p}_{< j}, \mathcal{I}_j = \text{ind2sub}([r_{j-1}, n_j], \mathbf{l}_{\leq j})$
 - 9: $\mathcal{I}_{\beta_j}^{\leq j} = (\mathcal{I}_{\mathbf{p}_{< j}(\beta_j)}^{\leq j-1}, \mathcal{I}_j(\beta_j))$, $\beta_j = 1, 2, \dots, s_j$
 - 10: **end for**
 - 11: $\mathcal{I}^{> d-1} = \text{DEIM}_{s_{d-1}}([\mathbf{K}_d^{(1)}]^T)$
 - 12: **for** $j = d - 2$ **to** 1 **do**
 - 13: $(\mathbf{W}_{j+1} \boldsymbol{\Sigma}_{j+1})^{(r)} = \mathbf{U}_j \boldsymbol{\Sigma}_j \mathbf{V}_{j+1}^{(r)}$
 - 14: $\mathbf{W}_j = \mathbf{W}_{j+1} \mathbf{U}_j$ ▷ TT-SVD (8) with $k = j$
 - 15: $\widehat{\mathbf{V}}_{> j}(i_{j+1} \beta_{j+1}, \alpha_j) = \mathbf{V}_{> j}(i_{j+1} \mathcal{I}_{\beta_{j+1}}^{> j+1}, \alpha_j)$ ▷ restrict right singular vectors
 - 16: $\mathbf{l}_{> j} = \text{DEIM}_{s_j}(\widehat{\mathbf{V}}_{> j})$
 - 17: $\mathcal{J}_{j+1}, \mathbf{p}_{> j+1} = \text{ind2sub}([n_j, r_j], \mathbf{l}_{> j})$
 - 18: $\mathcal{I}_{\beta_j}^{> j} = (\mathcal{J}_{j+1}(\beta_j), \mathcal{I}_{\mathbf{p}_{> j+1}(\beta_j)}^{> j+1})$, $\beta_j = 1, 2, \dots, s_j$
 - 19: **end for**
-

where $\mathbf{f}(\mathcal{I}^{\leq k-1}, :, \mathcal{I}^{> k})$ denotes $s_{k-1} \times n_k \times s_k$ tensor obtained by restricting \mathbf{f} to the s_{k-1} indices $\mathcal{I}^{\leq k-1}$ and the s_k indices $\mathcal{I}^{> k}$. Next, we show that every rank- r TT (5) is equal to a TT-cross interpolant with nested indices obtained with the TT-cross-DEIM. To do so, we first prove the following Lemma.

Lemma 2.1. *If the TT-rank of \mathbf{f} is equal to r and $\mathcal{I}^{\leq k}, \mathcal{I}^{> k}$ are $s_k \leq r_k$ indices obtained with the TT-cross-DEIM Algorithm 1 for all $k = 1, 2, \dots, d$, then the $s_k \times r_k$ matrices*

$$\mathbf{M}_k(\beta_k, \alpha_k) = \mathbf{W}_{\leq k}(\mathcal{I}_{\beta_k}^{\leq k}, \alpha_k), \quad \mathbf{N}_k(\beta_k, \alpha_k) = \mathbf{V}_{> k}(\mathcal{I}_{\beta_k}^{> k}, \alpha_k) \quad (29)$$

are full rank for all $k = 1, 2, \dots, d-1$.

Proof: We prove the result for \mathbf{M}_k by induction on k . Because the rank of \mathbf{f} is equal to r , the left unfolding $\mathbf{W}_1^{(l)}$ of the first core in the TT-SVD representation (8) with $k = 1$ is full rank. The s_1 indices $\mathcal{I}^{\leq 1}$ are obtained in (11) from $\mathbf{W}_1^{(l)}$ with the DEIM and invoking [30, Lemma 3.1] we have that the $s_1 \times r_1$ matrix $\mathbf{M}_1 = \mathbf{W}_{\leq 1}(\mathcal{I}^{\leq 1}, :)$ is full rank. This establishes the result for \mathbf{M}_k when $k = 1$. Now assume that \mathbf{M}_{k-1} is full rank and substitute \mathbf{M}_{k-1} into (18) to obtain

$$\widehat{\mathbf{W}}_k(\beta_{k-1} i_k, \alpha_k) = \sum_{\alpha_{k-1}=1}^{r_{k-1}} \mathbf{M}_{k-1}(\beta_{k-1}, \alpha_{k-1}) \mathbf{W}_k(\alpha_{k-1}, i_k, \alpha_k). \quad (30)$$

Because \mathbf{M}_{k-1} is full rank and both unfoldings of \mathbf{W}_k are full rank, it follows that $\widehat{\mathbf{W}}_k$ is full rank. In (19) we obtain s_k indices $\mathbf{l}_{\leq k}$ from $\widehat{\mathbf{W}}_k$ and once again invoking [30, Lemma 3.1] we have that the $s_k \times r_k$ matrix $\widehat{\mathbf{W}}_k(\mathbf{l}_{\leq k}, :)$ is full rank. The indices $\mathcal{I}^{\leq k}$ are obtained from $\mathbf{l}_{\leq k}$ in (15) so that

$$\mathbf{W}_{\leq k}(\mathcal{I}_{\beta_k}^{\leq k}, \alpha_k) = \widehat{\mathbf{W}}_{\leq k}(\mathbf{l}_{\leq k}(\beta_k), \alpha_k), \quad (31)$$

proving the result for \mathbf{M}_k . The statement for \mathbf{N}_k is proven with a similar argument inducting on descending values of k . \square

Theorem 2.1 (Exactness of TT-cross-DEIM). *Any rank- r tensor $\mathbf{f} \in \mathbb{R}^{n_1 \times \dots \times n_d}$ admits an exact rank- r tensor cross interpolant with nested indices obtained from the TT-cross-DEIM algorithm.*

Proof: First express the rank- r tensor \mathbf{f} in the TT format (5). Then apply the TT-cross-DEIM Algorithm 1 to the TT-cores in (5) with desired tensor cross interpolation rank r to obtain nested tensor cross indices $\{\mathcal{I}^{\leq k}, \mathcal{I}^{> k}\}$. Each $r_k \times r_k$ matrix $\mathbf{f}(\mathcal{I}^{\leq k}, \mathcal{I}^{> k})$ can be expressed as the product of \mathbf{M}_k and \mathbf{N}_k (see (29))

$$\mathbf{f}(\mathcal{I}^{\leq k}, \mathcal{I}^{> k}) = \mathbf{M}_k \mathbf{N}_k^T, \quad k = 1, 2, \dots, d-1. \quad (32)$$

According to Lemma 2.1, both \mathbf{M}_k and \mathbf{N}_k are invertible from which it follows that (32) is invertible. According to [12, Theorem 2], any collection of r_k indices $\mathcal{I}^{\leq k}, \mathcal{I}^{> k}$ for $k = 1, 2, \dots, d-1$ such that the $r_k \times r_k$ matrices (32) are invertible results in a tensor cross approximation (6) that is equal to \mathbf{f} . \square

When the rank s of the cross approximation (6) is less than the rank r of \mathbf{f} , it has been shown [26, Theorem 3] that the quality of the tensor cross approximation depends on the parameter

$$a = \max_{k=1, \dots, d-1} \left\{ \left\| \left[\mathbf{W}_{\leq k}(\mathcal{I}^{\leq k}, 1 : s_k) \right]^\dagger \right\|_F, \left\| \left[\mathbf{V}_{> k}(\mathcal{I}^{> k}, 1 : s_k) \right]^\dagger \right\|_F \right\}. \quad (33)$$

Here, $\mathbf{W}_{\leq k}(:, 1 : s_k)$ and $\mathbf{V}_{> k}(:, 1 : s_k)$ contain the first s_k left and right singular vectors of $\mathbf{f}^{(k)}$ (see (7)). To optimize the quality of the tensor cross approximation (6), the indices $\{\mathcal{I}^{\leq k}, \mathcal{I}^{> k}\}$ should be chosen to minimize (33). The proposed TT-cross-DEIM (Algorithm 1) utilizes the DEIM algorithm to obtain $\mathbf{l}_{\leq j}$ in (19) and $\mathbf{l}_{> j}$ in (25) from a greedy search that minimizes

$$\left\| \left[\widehat{\mathbf{W}}_{\leq j}(\mathbf{l}_{\leq j}, 1 : s_k) \right]^{-1} \right\|_F \quad \text{and} \quad \left\| \left[\widehat{\mathbf{V}}_{> k}(\mathbf{l}_{> k}, 1 : s_k) \right]^{-1} \right\|_F.$$

Given that $\widehat{\mathbf{W}}_{\leq k}(:, 1 : s_k)$ is the restriction of $\mathbf{W}_{\leq k}(:, 1 : s_k)$ to indices $\mathcal{I}^{\leq k-1}$ (see (18)) and $\widehat{\mathbf{V}}_{> k}(:, 1 : s_k)$ is the restriction of $\mathbf{V}_{> k}(:, 1 : s_k)$ to indices $\mathcal{I}^{> k+1}$ (see (24)), the proposed algorithm is designed select $\{\mathcal{I}^{\leq k}, \mathcal{I}^{> k}\}$ that minimize (33) subject to the constraint that the indices are nested (27).

3. Time integration on low-rank tensor manifolds

We now present a new method based on dynamical low-rank approximation to compute an approximate solution $\mathbf{f}(t)$ to the nonlinear differential equation (2) by enforcing (4) with indices obtained from Algorithm 1. The idea of dynamical low-rank approximation is to integrate $\mathbf{f}(t)$ on the fixed-rank tensor manifold [17]

$$\mathcal{M}_r = \{\mathbf{f} \in \mathbb{R}^{n_1 \times \dots \times n_d} \mid \text{TT-rank}(\mathbf{f}) = r\}, \quad (34)$$

by approximating $G(\mathbf{f}(t), t)$ with a tensor $d\mathbf{f}(t)/dt$ in the tangent space $T_{\mathbf{f}(t)}\mathcal{M}_r$ at each time t . For any tensor $\mathbf{f} \in \mathcal{M}_r$, we define the tangent space $T_{\mathbf{f}}\mathcal{M}_r$ as a collection of equivalence classes of velocities of smooth curves on \mathcal{M}_r passing through \mathbf{f}

$$T_{\mathbf{f}}\mathcal{M}_r = \{\gamma'(s)|_{s=0} \mid \gamma(s) \in C^1((-\delta, \delta), \mathcal{M}_r), \gamma(0) = \mathbf{f}\}, \quad (35)$$

and denote by

$$P_{\mathbf{f}} : \mathbb{R}^{n_1 \times \dots \times n_d} \rightarrow T_{\mathbf{f}}\mathcal{M}_r, \quad (36)$$

a projection onto the tangent space (35). If the initial condition \mathbf{u}_0 provided in (2) belongs to \mathcal{M}_r , then the solution to the tensor differential equation

$$\frac{d\mathbf{f}(t)}{dt} = P_{\mathbf{f}(t)}(G(\mathbf{f}(t), t)), \quad \mathbf{f}(0) = \mathbf{u}_0, \quad (37)$$

is a low-rank approximation of the solution to (2) that remains on \mathcal{M}_r for all t . Traditionally, dynamical low-rank methods employ an orthogonal projection $\hat{P}_{\mathbf{f}} : \mathbb{R}^{n_1 \times \dots \times n_d} \rightarrow T_{\mathbf{f}}\mathcal{M}_r$ onto the tangent space, which minimizes the Frobenius norm of the residual (3) (see Figure 1) but is often expensive to compute for nonlinear differential equations. We propose a new dynamical low-rank method that employs an interpolatory projection onto the tangent space, which ensures that the residual vanishes (4) at a set of indices $\{\mathcal{I}^{\leq k}, \mathcal{I}^{> k}\}$ selected at each time t . Such interpolatory projection is sub-optimal with respect to the Frobenius norm but is efficient to compute for nonlinear G .

3.1. Interpolatory projection onto the tangent space

To define the interpolatory projection, we first show the existence and uniqueness of interpolatory tangent tensors. We provide the proof in Appendix A.

Theorem 3.1. *Suppose $\mathbf{f} \in \mathcal{M}_r$ is represented exactly as a tensor cross interpolant with indices $\{\mathcal{I}^{\leq k}, \mathcal{I}^{> k}\}$. For any $\mathbf{X} \in \mathbb{R}^{n_1 \times \dots \times n_d}$, there exists a unique element $\delta\mathbf{f} \in T_{\mathbf{f}}\mathcal{M}_r$ satisfying*

$$\delta\mathbf{f}(\mathcal{I}^{\leq k-1}, :, \mathcal{I}^{> k}) = \mathbf{X}(\mathcal{I}^{\leq k-1}, :, \mathcal{I}^{> k}), \quad k = 1, 2, \dots, d.$$

Given a set of nested indices $\{\mathcal{I}^{\leq k}, \mathcal{I}^{> k}\}$ that provide a tensor cross interpolant of \mathbf{f} (e.g., indices obtained from Algorithm 1), we define the interpolatory tangent space projection (36) by requiring

$$(P_{\mathbf{f}}\mathbf{X})(\mathcal{I}^{\leq k-1}, :, \mathcal{I}^{> k}) = \mathbf{X}(\mathcal{I}^{\leq k-1}, :, \mathcal{I}^{> k}), \quad k = 1, 2, \dots, d. \quad (38)$$

According to Theorem 3.1, the conditions (38) identify a unique tensor $P_{\mathbf{f}}\mathbf{X}$ in the tangent space (35). Utilizing (38) in the dynamical low-rank evolution equation (37) yields the system of equations

$$\frac{d\mathbf{f}(\mathcal{I}^{\leq k-1}(t), :, \mathcal{I}^{> k}(t); t)}{dt} = \mathbf{G}(\mathcal{I}^{\leq k-1}(t), :, \mathcal{I}^{> k}(t); t), \quad k = 1, 2, \dots, d, \quad (39)$$

where $\mathbf{G}(t) = G(\mathbf{f}(t), t)$. Note that the system of equations (39) is equivalent to (4), i.e., dynamical low-rank approximation with the interpolatory tangent space projection (38) ensures that the residual (3) vanishes at the selected interpolation indices. In order to advance the solution $\mathbf{f}(t)$ to (37) on \mathcal{M}_r , we integrate the system of equations (39) forward in time. If G arises from the spatial discretization of a PDE (1) involving differential operators, then evaluating $\mathbf{G}(\mathcal{I}^{\leq k-1}, :, \mathcal{I}^{> k})$ requires entries of \mathbf{f} at indices adjacent to $\{\mathcal{I}^{\leq k}, \mathcal{I}^{> k}\}$. We denote by $\mathcal{I}_{(a)}^{\leq k}$ ($\mathcal{I}_{(a)}^{> k}$) the union of $\mathcal{I}^{\leq k}$ ($\mathcal{I}^{> k}$) with the required adjacent indices, and compute the right-hand side tensors in (39) by

$$\mathbf{G}(\mathcal{I}^{\leq k-1}, :, \mathcal{I}^{> k}; t) = \mathbf{G}\left(\mathbf{f}\left(\mathcal{I}_{(a)}^{\leq k-1}, :, \mathcal{I}_{(a)}^{> k}; t\right), t\right), \quad k = 1, 2, \dots, d. \quad (40)$$

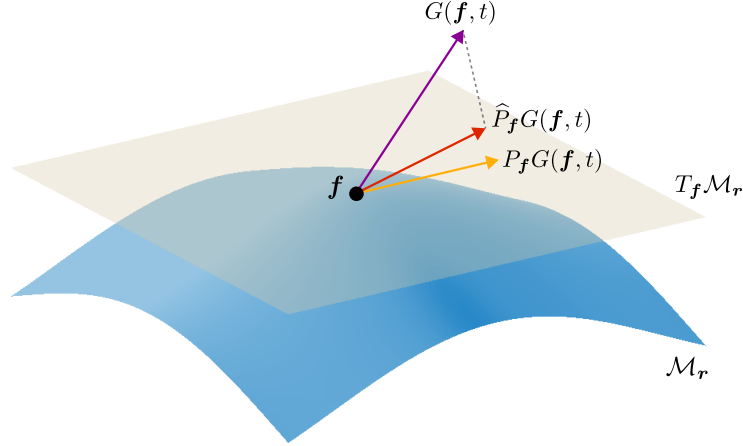


Figure 1: A sketch of the low-rank tensor manifold \mathcal{M}_r and its tangent space $T_f \mathcal{M}_r$ at the point $\mathbf{f} \in \mathcal{M}_r$. Also shown is a tensor \mathbf{X} that does not belong to the tangent space $T_f \mathcal{M}_r$, and its orthogonal projection $\hat{P}_f \mathbf{X}$ and interpolatory projection $P_f \mathbf{X}$ onto the tangent space $T_f \mathcal{M}_r$. The orthogonal projection is optimal with respect to the Frobenius norm but expensive to compute for nonlinear G while the interpolatory projection is sub-optimal in the Frobenius norm but efficient to compute for nonlinear G .

We can efficiently calculate (40) for many functions G that involve nonlinearities or coefficient tensors that are not low-rank. In such cases, the system of equations (39) provides a clear computational advantage over the dynamical low-rank evolution equations obtained from orthogonal projection onto the tangent space $T_{\mathbf{f}(t)} \mathcal{M}_r$. The latter equations involve inner products between \mathbf{G} and the TT-cores of $\mathbf{f}(t)$ (see, e.g., [21, Section 3]). To efficiently compute these inner products it is necessary to obtain a low-rank representation of \mathbf{G} , which can be challenging to compute when G includes nonlinearities or coefficient tensors that are not available in a low-rank format. In addition, the evolution equations obtained from orthogonal projection onto the tangent space involve inverse auto-correlation matrices that become ill-conditioned when small singular values are present in the low-rank solution. In order to obtain a robust numerical scheme from such evolution equations it is necessary to use operator splitting [21] or unconventional [3] time integration schemes.

3.2. Constructing the low-rank solution in TT format

The dynamical low-rank evolution equations (39) obtained from interpolatory projection onto the tangent space (38) do not suffer from ill-conditioned matrices. However, constructing $\mathbf{f}(t)$ in the TT format from the solution to (39) using cross interpolation

$$\mathbf{f}(i_1, \dots, i_d; t) = \prod_{k=1}^d \mathbf{f}(\mathcal{I}^{\leq k-1}(t), i_k, \mathcal{I}^{> k}(t); t) [\mathbf{f}(\mathcal{I}^{\leq k}(t), \mathcal{I}^{> k}(t); t)]^{-1}, \quad (41)$$

involves inverses of the $r_k \times r_k$ (time-dependent) matrices $\mathbf{S}_k(t) = \mathbf{f}(\mathcal{I}^{\leq k}, \mathcal{I}^{> k}; t)$, which may be ill-conditioned. Instead of inverting these matrices directly, we propose a more robust method for computing $\mathbf{f}(t)$ as follows. First we obtain the $r_k \times r_k$ matrices $\mathbf{f}(\mathcal{I}^{\leq k}, \mathcal{I}^{> k}; t)$ whose inverse appears in (41), by finding a set of indices $\mathbf{p}_{< k}$ for each $k = 1, 2, \dots, d-1$ that satisfies

$$\mathcal{I}_{\mathbf{p}_{< k}(\alpha_k)}^{\leq k-1} = \mathcal{I}_{\alpha_k}^{\leq k}(1 : k-1), \quad \alpha_k = 1, 2, \dots, r_k.$$

The indices $\mathbf{p}_{< k}$ exist because $\{\mathcal{I}^{\leq k}, \mathcal{I}^{> k}\}$ are nested (27). We can then evaluate the desired matrices using the solution to (39)

$$\begin{aligned} \mathbf{S}_k(\alpha_k, \alpha'_k; t) &= \mathbf{f}\left(\mathcal{I}_{\alpha_k}^{\leq k}, \mathcal{I}_{\alpha'_k}^{> k}; t\right) \\ &= \mathbf{f}\left(\mathcal{I}_{\mathbf{p}_{< k}(\alpha_k)}^{\leq k-1}, \mathcal{I}_{\alpha_k}^{\leq k}(k), \mathcal{I}_{\alpha'_k}^{> k}; t\right), \quad \alpha_k, \alpha'_k = 1, 2, \dots, r_k. \end{aligned} \quad (42)$$

Instead of inverting the matrices (42) as written in (41), we obtain a more robust procedure for computing $\mathbf{f}(t)$ by taking QR-decompositions

$$\mathbf{f}(\mathcal{I}^{\leq k-1}, :, \mathcal{I}^{> k})^{(l)} = \mathbf{Q}_k^{(l)} \mathbf{R}_k, \quad k = 1, 2, \dots, d-1, \quad (43)$$

to rewrite (42) as

$$\mathbf{S}_k(\alpha_k, \alpha'_k) = \mathbf{Q}_k(\mathbf{p}_{< k}(\alpha_k), \mathcal{I}_{\alpha_k}^{\leq k}(k), :) \mathbf{R}_k(:, \alpha'_k), \quad \alpha_k, \alpha'_k = 1, 2, \dots, r_k, \quad (44)$$

where we dropped the dependence on t to simplify the notation. Then substituting (43)-(44) into (41) we obtain

$$\begin{aligned} \mathbf{f}(i_1, \dots, i_d; t) &= \prod_{k=1}^d \mathbf{Q}_k(i_k) \mathbf{R}_k [\mathbf{Q}_k(\mathbf{p}_{< k}, \mathcal{I}^{\leq k}(k), :) \mathbf{R}_k]^{-1} \\ &= \prod_{k=1}^d \mathbf{Q}_k(i_k) \mathbf{U}_k^{-1}, \end{aligned} \quad (45)$$

where

$$\mathbf{U}_k(\alpha_k, \alpha'_k) = \mathbf{Q}_k(\mathbf{p}_{< k}(\alpha_k), \mathcal{I}_{\alpha_k}^{\leq k}(k), \alpha'_k), \quad \alpha_k, \alpha'_k = 1, 2, \dots, r_k. \quad (46)$$

Computing $\mathbf{f}(t)$ via (45) instead of (41) yields a more stable numerical algorithm as the matrices $\mathbf{Q}_k(\mathbf{p}_{< k}, \mathcal{I}^{\leq k}(k), i_k)$ are better conditioned than $\mathbf{f}(\mathcal{I}^{\leq k}, \mathcal{I}^{> k})$. The improvement in condition number is indeed verified by our numerical experiments as shown in Figure 2(d).

3.3. Discrete-time dynamical low-rank collocation integrator

To describe one step of the proposed dynamical low-rank integrator, let us discretize the time domain $[0, T]$ into $N + 1$ evenly spaced time instants

$$t_j = j\Delta t, \quad \Delta t = \frac{T}{N}, \quad j = 0, 1, \dots, N, \quad (47)$$

and assume at time t_j the approximate low-rank solution $\mathbf{f}(t_j) \in \mathcal{M}_r$ is expressed in the TT format

$$\mathbf{f}(t_j) = \mathbf{C}_1(t_j) \mathbf{C}_2(t_j) \cdots \mathbf{C}_d(t_j). \quad (48)$$

Applying Algorithm 1 to (48) we obtain indices $\{\mathcal{I}^{\leq k}(t_j), \mathcal{I}^{> k}(t_j)\}$, which by Theorem 2.1 provide an exact representation of $\mathbf{f}(t_j)$ as a tensor cross interpolant (41). To advance the solution forward on \mathcal{M}_r , we take one step of the system (39) using a explicit time stepping scheme, e.g., Euler forward yields

$$\begin{aligned} &\mathbf{f}(\mathcal{I}^{\leq k-1}(t_j), :, \mathcal{I}^{> k}(t_j); t_{j+1}) \\ &= \mathbf{f}(\mathcal{I}^{\leq k-1}(t_j), :, \mathcal{I}^{> k}(t_j); t_j) + \Delta t \mathbf{G}(\mathcal{I}^{\leq k-1}(t_j), :, \mathcal{I}^{> k}(t_j); t_j), \quad k = 1, 2, \dots, d. \end{aligned} \quad (49)$$

Higher order explicit time stepping schemes are also possible, e.g., Adams-Bashforth 2

$$\begin{aligned} &\mathbf{f}(\mathcal{I}^{\leq k-1}(t_j), :, \mathcal{I}^{> k}(t_j); t_{j+1}) \\ &= \mathbf{f}(\mathcal{I}^{\leq k-1}(t_j), :, \mathcal{I}^{> k}(t_j); t_j) + \frac{3}{2} \Delta t \mathbf{G}(\mathcal{I}^{\leq k-1}(t_j), :, \mathcal{I}^{> k}(t_j); t_j) \\ &\quad - \frac{1}{2} \Delta t \mathbf{G}(\mathcal{I}^{\leq k-1}(t_j), :, \mathcal{I}^{> k}(t_j); t_{j-1}), \quad k = 1, 2, \dots, d. \end{aligned} \quad (50)$$

Note that the tensor cross indices in these explicit time-stepping schemes are those computed at time t_j from $\mathbf{f}(t_j)$ with Algorithm 1. Using the result of explicit time integration (49) (or (50)), we construct TT-cores for the solution at time t_{j+1}

$$\mathbf{f}(t_{j+1}) = \mathbf{C}_1(t_{j+1}) \mathbf{C}_2(t_{j+1}) \cdots \mathbf{C}_d(t_{j+1}), \quad (51)$$

using the procedure described in (42)-(45), i.e.,

$$\begin{aligned} \mathbf{C}_k(t_{j+1}) &= \mathbf{Q}_k \mathbf{U}_k^{-1}, \quad k = 1, 2, \dots, d-1, \\ \mathbf{C}_d(t_{j+1}) &= \mathbf{f}(\mathcal{I}^{\leq d-1}(t_j), :, \mathcal{I}^{> d}(t_j); t_{j+1}). \end{aligned} \quad (52)$$

This completes one step of the dynamical low-rank collocation integrator. To perform the next time integration step from t_{j+1} to t_{j+2} , new indices $\{\mathcal{I}^{\leq k}(t_{j+1}), \mathcal{I}^{> k}(t_{j+1})\}$ may be computed from the TT-representation (51) with Algorithm 1. However it may not be necessary to compute new indices at every time step as indices can be used for multiple time steps, provided the condition number of the matrices \mathbf{U}_k in (52) is small.

3.4. Rank-adaptive time integration

The solution to (2) is often not accurately represented on a tensor manifold \mathcal{M}_r with constant rank for all $t \in [0, T]$. Therefore, the dynamical low-rank integrator must be able to decrease or increase the rank of the solution manifold as necessary. While performing one time step of the proposed dynamical low-rank collocation integrator, the solution rank can be easily decreased or increased. To decrease the solution rank, we use the TT-SVD truncation algorithm at each time t with no additional computational cost to the integrator. Indeed, as we mentioned in Section 2, all TT-SVD representations of the solution required for TT-SVD truncation are computed in the TT-cross-DEIM index selection Algorithm 1.

To increase the k th component of the TT solution rank using Algorithm 1, we sample $\hat{r}_k > r_k$ indices $\mathbf{l}_{\leq k}$ from the left singular vectors (19) and $\hat{r}_k > r_k$ indices $\mathbf{l}_{> k}$ from right singular vectors in (25). The DEIM index selection algorithm only samples as many indices as singular vectors. To sample additional indices, we augment the DEIM indices with additional indices selected by another sparse index selection algorithm, e.g., GappyPOD+E [25]. From the $\mathbf{l}_{\leq k}, \mathbf{l}_{> k}$ we construct $\mathcal{I}^{\leq k}, \mathcal{I}^{> k}$ in (20),(26) each with \hat{r}_k indices. We then integrate the solution $\mathbf{f}(t)$ forward in time on the manifold $\mathcal{M}_{\hat{r}}$ using the equations (39). It is well-known that the solution $\mathbf{f}(t)$ with rank r belongs to the boundary of the higher rank manifold $\mathcal{M}_{\hat{r}}$, where the tangent space is not well-defined [31]. Nevertheless, the evolution equations (39), which define the interpolatory tangent space projection (36), are well-defined on the boundary of $\mathcal{M}_{\hat{r}}$. These equations allow us to integrate $\mathbf{f}(t)$ forward in time on $\mathcal{M}_{\hat{r}}$ thereby increasing the solution rank.

A simple criterion for determining if the k th component of the TT-rank vector should be increased at time t is based on the size of the smallest singular value in the SVD (7) normalized by the Frobenius norm of $\mathbf{f}^{(k)}$

$$\epsilon_k(t) = \frac{\sigma_k(r_k, t)}{\sqrt{\sum_{\alpha_k=1}^{r_k} \sigma_k(\alpha_k, t)^2}}, \quad k = 1, 2, \dots, d-1. \quad (53)$$

The k th component of the rank r_k can be selected at each time t to ensure that $\epsilon_k(t)$ remains in a desired range $\epsilon_l \leq \epsilon_k(t) \leq \epsilon_u$. This criterion is an adaptation of the rank-adaptive criterion introduced in [13] for matrix differential equations and subsequently generalized to the Tucker format [15], to the TT format.

4. Numerical examples

We now apply the proposed dynamical low-rank collocation integrator to tensor differential equations (2) arising from the discretization of partial differential equations (1) and compare the results with existing time integration schemes on tensor manifolds.

4.1. Allen-Cahn equation

The Allen-Cahn equation is a reaction-diffusion PDE that models phase separation in multi-component alloy systems [1, 18]. A simple form of such equation includes a Laplacian and a cubic non-linearity

$$\begin{cases} \frac{\partial u(\mathbf{x}, t)}{\partial t} = \alpha \Delta u(\mathbf{x}, t) + u(\mathbf{x}, t) - u(\mathbf{x}, t)^3, \\ u(\mathbf{x}, 0) = u_0(\mathbf{x}). \end{cases} \quad (54)$$

We consider the spatial domain $\Omega = [0, 2\pi]^3$ with periodic boundary conditions, initial condition $u_0(x_1, x_2, x_3) = g(x_1, x_2, x_3) - g(2x_1, x_2, x_3) + g(x_1, 2x_2, x_3) - g(x_1, x_2, 2x_3)$ where

$$g(x_1, x_2, x_3) = \frac{\left(e^{-\tan(x_1)^2} + e^{-\tan(x_2)^2} + e^{-\tan(x_3)^2} \right) \sin(x_1 + x_2 + x_3)}{1 + e^{|\csc(-x_1/2)|} + e^{|\csc(-x_2/2)|} + e^{|\csc(-x_3/2)|}}, \quad (55)$$

and diffusion parameter $\alpha = 0.1$. Discretizing Ω using $n = 64$ points in each dimension and approximating derivatives with a Fourier pseudo-spectral method [16], we obtain a semi-discrete version of the Allen-Cahn equation in the form of (2). To assess the accuracy of the proposed low-rank tensor integrator, we computed a reference solution \mathbf{f}_{ref} by integrating the full tensor solution (64^3 degrees of freedom) to the semi-discrete equation with the four-stage explicit Runge-Kutta (RK4) method using time step-size $\Delta t = 10^{-3}$.

We computed three approximate low-rank solutions on a TT manifold (34) with the step-truncation SVD method (ST-SVD) [28] using three different relative truncation tolerances $\delta = 10^{-4}, 10^{-6}, 10^{-10}$. We then computed three approximate low-rank solutions on the TT manifold using the proposed dynamical low-rank collocation (DLR-c) integrator. In order to compare the results with the ST-SVD simulations, we set the solution rank in the DLR-c simulations equal to the ranks obtained from the ST-SVD simulations with truncation tolerances $\delta = 10^{-4}, 10^{-6}, 10^{-10}$. We performed the rank decrease using TT-SVD truncation, and the rank increase by sampling more tensor cross indices than singular vectors using the GappyPOD+E algorithm [25] as described in Section 3.4. Time integration was performed in the ST-SVD and DLR-c simulations with Adams-Bashforth 2 and step-size $\Delta t = 10^{-3}$.

4.1.1. Rank, error and stability

In Figure 2(b), we plot the 1-norm of the TT solution rank versus time for each low-rank simulation. We observe that the smoothing effects due to diffusion in the Allen-Cahn equation cause the TT ranks to decay relatively quickly from time $t = 0$ to time $t \approx 1.5$. In Figure 2(a), we plot the relative error measured in the Frobenius norm versus time for each ST-SVD and DLR-c simulation. The ST-SVD solution is more accurate than the DLR-c solution computed with the same rank, which is expected. Indeed, the ST-SVD method computes the best rank- r projection of the solution onto the low-rank manifold \mathcal{M}_r at each time step. In contrast, the DLR-c method computes a sub-optimal projection (measured in the Frobenius norm) onto the tangent space of the low-rank manifold at each time step. When the rank of the TT solutions is large enough, in this case corresponding to $\delta = 10^{-10}$, the error due to time integration dominates the low-rank approximation error, and the ST-SVD and DLR-c methods produce solutions with the same accuracy. In Figure 2(c), we compare the accuracy of the interpolatory projection (i-proj) onto the tangent space (computed from the DLR-c simulation) and the orthogonal projection (o-proj) onto the tangent space (computed from the ST-SVD simulation). The orthogonal projection is more accurate than the interpolatory projection by approximately one order of magnitude or less at each time t and both errors follow the same trend for all $t \in [0, 10]$. To assess the stability of the proposed DLR-c method, in Figure 2(d) we plot the condition number of the $r_k \times r_k$ matrices (42) and (46) versus time that are used to construct the solution in TT format at each time step. We observe that the orthogonalization procedure described in (43)-(46) results in a more stable numerical scheme integration scheme.

4.1.2. Computational cost

As we mentioned previously, the ST-SVD method and the orthogonal projection onto the tangent space of \mathcal{M}_r require the right-hand side tensor $G(\mathbf{f}, t)$ of (2) in a low-rank format. In the case of the Allen-Cahn equation (54), G includes a cubic nonlinearity that can make computing $G(\mathbf{f}, t)$ in a low-rank format expensive. Indeed, recall that standard algorithms for multiplying two TTs \mathbf{f}_1 and \mathbf{f}_2 with ranks $\mathbf{r}_1 = [r_1 \ \cdots \ r_1]$ and $\mathbf{r}_2 = [r_2 \ \cdots \ r_2]$ results in a TT $\mathbf{f}_1 \mathbf{f}_2$ with (non-optimal) rank equal to the Hadamard (element-wise) product of the two ranks $\mathbf{r}_1 \circ \mathbf{r}_2$ that must be truncated. Performing such truncation with the TT-SVD algorithm requires $\mathcal{O}(dn(r_1 r_2)^3)$ FLOPS. We used two TT-SVD truncations \mathfrak{T}_δ with relative accuracy δ to compute the cubic term

$$(\mathbf{f})^3 = \mathfrak{T}_\delta^{\text{svd}}(\mathbf{f} \mathfrak{T}_\delta^{\text{svd}}(\mathbf{f} \mathbf{f})), \quad (56)$$

in (54). Therefore, the computation of the right-hand side tensor $G(\mathbf{f}, t)$ of the discretized Allen-Cahn equation (54), which is required for ST-SVD and dynamical low-rank using orthogonal projections, requires $\mathcal{O}(dnr^6)$ FLOPS. It is possible to accelerate the computation $G(\mathbf{f}, t)$ by carrying out sums and products of TTs with approximate low-rank tensor arithmetic [20], black-box tensor cross approximation [12], or randomized algorithms [6]. However, such algorithms introduce additional errors in the low-rank approximation that can be difficult to control. The proposed DLR-c method does not require $G(\mathbf{f}, t)$ in a low-rank form and instead evaluates $G(\mathbf{f}, t)$ at dnr^2 indices (assuming the solution rank vector is constantly equal to r). These indices are computed with the TT-cross-DEIM (Algorithm 1) in $\mathcal{O}(dnr^3)$ FLOPS at each time step. Thus, the DLR-c integrator for (54) is significantly faster than the TT-SVD algorithm or dynamical low-rank approximation using orthogonal tangent space projection.

4.2. Fokker-Planck equation

The Fokker-Planck equation [27] describes the evolution of the probability density function (PDF) of state vector solving the Itô stochastic differential equation

$$d\mathbf{X}_t = \boldsymbol{\mu}(\mathbf{X}_t, t)dt + \boldsymbol{\sigma}(\mathbf{X}_t, t)dW_t, \quad (57)$$

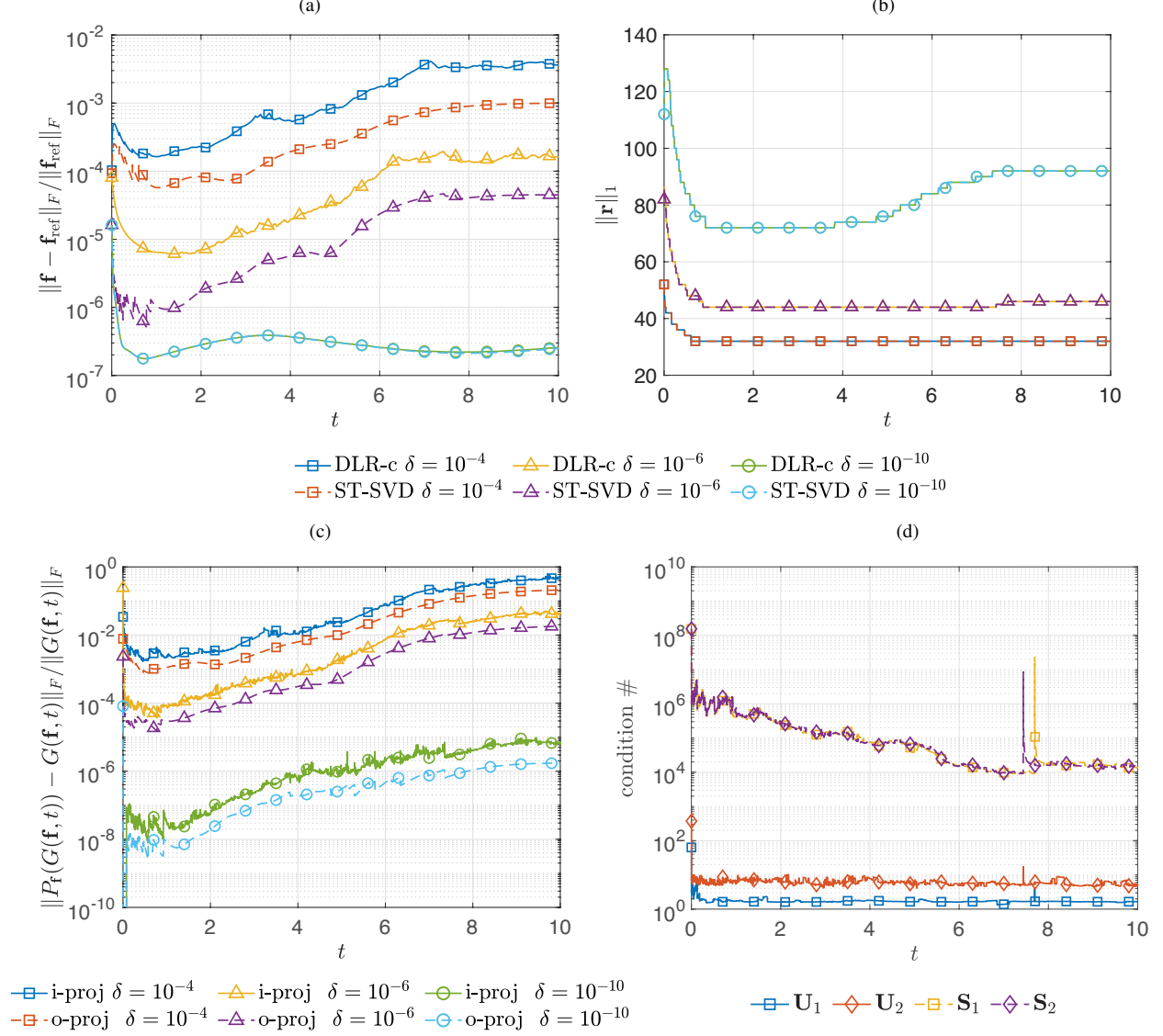


Figure 2: Low-rank approximations to the three-dimensional Allen-Cahn equation (54) computed with the DLR-c and ST-SVD integrators with ranks determined using different truncation tolerances $\delta = 10^{-4}, 10^{-6}, 10^{-10}$ in the ST-SVD method. (a) Relative error in the Frobenius norm versus time. (b) 1-norm of the TT-rank vector versus time. (c) Relative error of interpolatory (i-proj) and orthogonal (o-proj) projections onto the low-rank manifold tangent space versus time. (d) Condition number of the matrices orthogonalized matrices (46) used to construct the DLR-c solution in TT format and the non-orthogonalized matrices (42) versus time.

where \mathbf{X}_t is the d -dimensional state vector, $\boldsymbol{\mu}(\mathbf{X}_t, t)$ is the d -dimensional drift, $\boldsymbol{\sigma}(\mathbf{X}_t, t)$ is a $d \times m$ matrix and \mathbf{W}_t is an m -dimensional standard Wiener process. The Fokker-Planck equation corresponding to (57) takes the form

$$\begin{cases} \frac{\partial p(\mathbf{x}, t)}{\partial t} = \mathcal{L}(\mathbf{x}, t)p(\mathbf{x}, t), \\ p(\mathbf{x}, 0) = p_0(\mathbf{x}), \end{cases} \quad (58)$$

where $p_0(\mathbf{x})$ is the PDF of the initial state \mathbf{X}_0 , \mathcal{L} is a second-order linear differential operator defined by

$$\mathcal{L}(\mathbf{x}, t)p(\mathbf{x}, t) = - \sum_{i=1}^d \frac{\partial}{\partial x_i} (\boldsymbol{\mu}_i(\mathbf{x}, t)p(\mathbf{x}, t)) + \sum_{i,j=1}^d \frac{\partial^2}{\partial x_i \partial x_j} (\mathbf{D}_{ij}(\mathbf{x}, t)p(\mathbf{x}, t)), \quad (59)$$

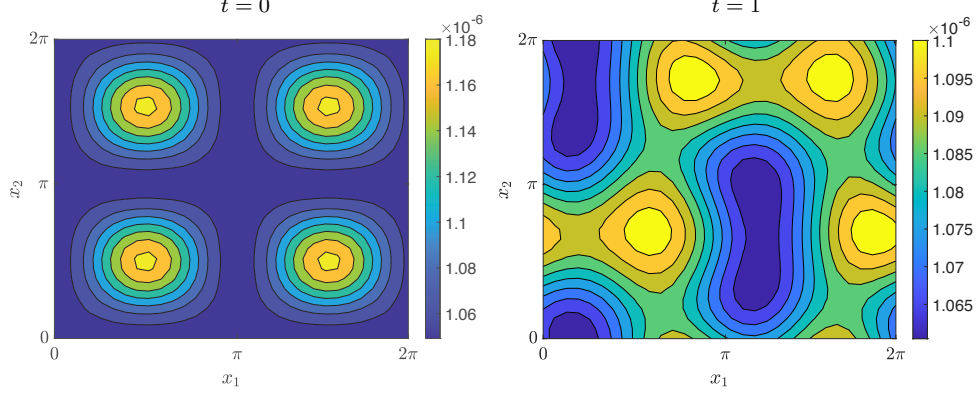


Figure 3: The (x_1, x_2) -marginal PDFs of the reference solution to the four-dimensional Fokker-Planck equation (58) at time $t = 0$ and $t = 1$.

and $D(\mathbf{x}, t) = \boldsymbol{\sigma}(\mathbf{x}, t)\boldsymbol{\sigma}(\mathbf{x}, t)^T/2$ is the diffusion tensor. For our numerical demonstration we consider the spatial domain $\Omega = [0, 2\pi]^4$ with periodic boundary conditions and set

$$p_0(\mathbf{x}) = \exp(\sin(x_1) \sin(x_2) \sin(x_3) \sin(x_4)), \quad (60)$$

and

$$\boldsymbol{\mu}(\mathbf{x}) = \frac{1}{2} \begin{bmatrix} g(x_2, x_3) \\ g(x_3, x_4) \\ g(x_4, x_1) \\ g(x_2, x_3) \end{bmatrix}, \quad \boldsymbol{\sigma}(\mathbf{x}) = \frac{1}{2} \begin{bmatrix} 1 & 0 & 0 & 0 \\ 0 & 1 & 0 & 0 \\ 0 & 0 & 1 & 0 \\ 0 & 0 & 0 & 1 \end{bmatrix}, \quad (61)$$

where $g(x, y) = \exp(\sin(x) \cos(y))$. With the drift and diffusion matrices chosen in (61), the operator (59) takes the form

$$\mathcal{L} = -\frac{1}{2} \left(g(x_2, x_3) \frac{\partial}{\partial x_1} + g(x_3, x_4) \frac{\partial}{\partial x_2} + g(x_4, x_1) \frac{\partial}{\partial x_3} + g(x_2, x_3) \frac{\partial}{\partial x_4} \right) + \frac{1}{2} \Delta. \quad (62)$$

Discretizing Ω using $n = 32$ points in each dimension and approximating derivatives with a Fourier pseudo-spectral method [16], we obtain a semi-discrete version of the Fokker-Planck equation in the form of (2). To assess the accuracy of the proposed low-rank tensor integrator, we computed a reference solution \mathbf{f}_{ref} by integrating the full tensor solution (32^4 degrees of freedom) to the semi-discrete equation with the four-stage explicit RK4 method using time step-size $\Delta t = 10^{-3}$. In Figure 3, we plot the (x_1, x_2) -marginal PDFs of the reference solution the four-dimensional Fokker-Planck equation (58) at time $t = 0$ and $t = 1$.

We computed two approximate low-rank solutions on a TT manifold (34) with the step-truncation SVD method (ST-SVD) [28] using different relative truncation tolerances $\delta = 10^{-6}, 10^{-8}$. Computing the ST-SVD simulation requires a low-rank approximation of $G(\mathbf{f}, t)$ at each time t . The map G obtained from discretizing (58) is linear and has four coefficient tensors $\mathbf{c}_1, \mathbf{c}_2, \mathbf{c}_3, \mathbf{c}_4 \in \mathbb{R}^{n \times n \times n \times n}$ (resulting from the discretization of $g(x, y)$) that are not expressed in a low-rank format upon discretization of G . In order to compute $G(\mathbf{f}, t)$ in low-rank format at each time, we decomposed the four coefficient tensors in G using TT-SVD compression with relative accuracy δ . For $\delta = 10^{-6}$ and $\delta = 10^{-8}$ we obtained coefficient tensors of the same rank

$$\begin{aligned} \text{TT-rank}(\mathbf{c}_1) &= [1 \quad 1 \quad 12 \quad 1 \quad 1], \\ \text{TT-rank}(\mathbf{c}_2) &= [1 \quad 1 \quad 1 \quad 12 \quad 1], \\ \text{TT-rank}(\mathbf{c}_3) &= [1 \quad 13 \quad 13 \quad 13 \quad 1], \\ \text{TT-rank}(\mathbf{c}_4) &= [1 \quad 1 \quad 12 \quad 1 \quad 1]. \end{aligned} \quad (63)$$

We computed $G(\mathbf{f}, t)$ in the ST-SVD method at each time step by taking products of the low-rank approximate coefficient tensors \mathbf{c}_k with the low-rank solution tensor \mathbf{f} and then used TT-SVD truncation to compress the product. We also applied TT-SVD truncation after adding two low-rank tensors in order to control tensor rank while computing $G(\mathbf{f}, t)$. Time integration for the ST-SVD simulation was performed with AB2 and time step-size $\Delta t = 10^{-3}$. In

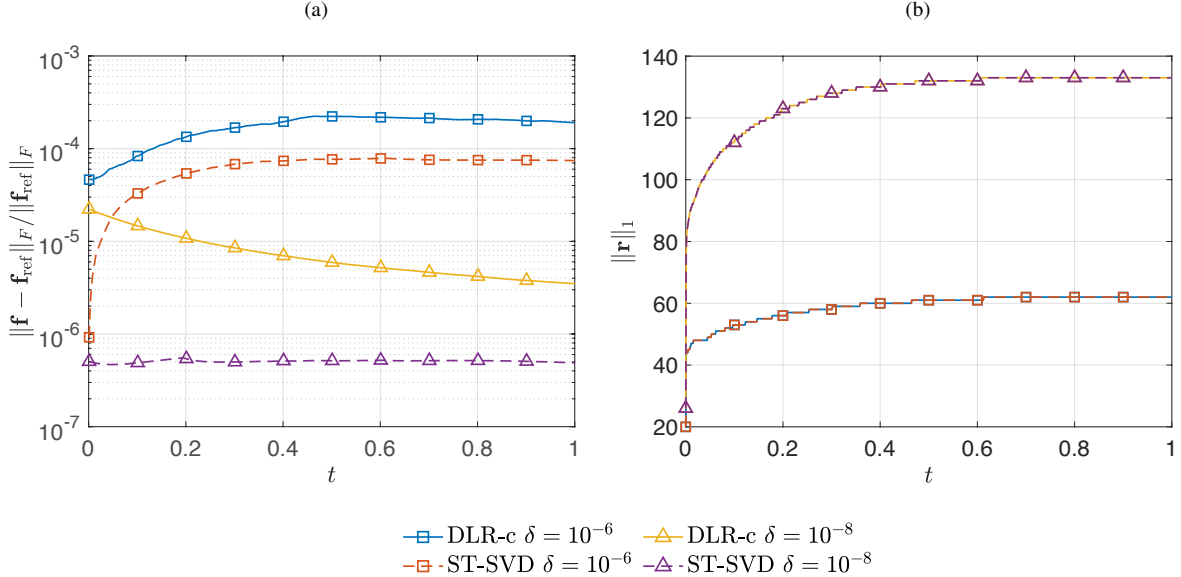


Figure 4: Low-rank approximations to the four-dimensional Fokker-Planck equation (58) computed with the DLR-c and ST-SVD integrators with ranks determined using different truncation tolerances $\delta = 10^{-6}, 10^{-8}$ in the ST-SVD method. (a) Relative error in the Frobenius norm versus time. (b) 1-norm of the TT-rank vector versus time.

Figure 4(b) we plot the 1-norm of the TT-rank of each ST-SVD solution versus time. We observe that the ranks of both solution increase until around $t = 0.5$ and then stabilize for $t \in [0.5, 1]$.

We then computed two approximate low-rank solutions on the TT manifold \mathcal{M}_r using the proposed dynamical low-rank collocation (DLR-c) integrator. Once again, in order to compare the results with the ST-SVD simulations, we set the solution ranks in the DLR-c simulations equal to the ranks obtained from the ST-SVD simulations with truncation tolerances $\delta = 10^{-6}, 10^{-8}$. We computed the right-hand side of the dynamical low-rank collocation evolution equations (39) by simply evaluating the coefficient tensors at the indices determined by the TT-cross-DEIM Algorithm at each time step. Unlike the ST-SVD method, the DLR-c method does not require computing low-rank approximations of the coefficient tensors in G and taking products of low-rank tensors that must then be truncated. Computing the orthogonal projection onto the tangent space in this case requires approximating the coefficient tensors of G in a low-rank format and then taking inner products between these tensors, which can be done efficiently (without constructing tensors of non-optimal rank) but is a highly intrusive process. In Figure 4(a) we compare the relative error in the Frobenius norm of the DLR-c solutions and the ST-SVD solutions computed with the same rank. We observe that for the same rank, the DLR-c solutions are less accurate than the ST-SVD solutions and closely follow the same trend. Once again, this is expected because the ST-SVD method computes the best rank- r projection of the solution onto the low-rank manifold \mathcal{M}_r at each time step, while the DLR-c method computes a sub-optimal projection onto the tangent space of the low-rank manifold at each time step.

5. Conclusions

We presented a new method for computing the solution to a nonlinear tensor differential equation on a low-rank manifold. The method relies on dynamical low-rank approximation, which involves integrating the approximate solution by projecting the differential equation onto a low-rank tangent space at each time. Traditionally, dynamical low-rank methods have employed an orthogonal projection onto the tangent space, which poses a significant computational challenge for nonlinear differential equations. To overcome this challenge, we proposed a new interpolatory projection onto the tangent space that satisfies the equation at a set of indices. To choose these indices, we introduced a new algorithm based on the DEIM that parameterizes the low-rank solution and its tangent space with tensor cross interpolants at each time. Our numerical experiments demonstrate that the interpolatory projection onto the tangent space provides a reasonable approximation of the tensor differential equation in the Frobenius norm that we can efficiently compute for nonlinear differential equations. Consequently, integrating the low-rank solution on \mathcal{M}

using the tangent tensor obtained from interpolatory projection yields a reasonable approximation to the solution in the Frobenius norm. The proposed method overcomes significant computational limitations of existing methodologies for time integration on low-rank tensor manifolds and facilitates the application of dynamical low-rank approximation to a broad class of nonlinear tensor differential equations.

Acknowledgements

This material is based upon work supported by the U.S. Department of Energy, Office of Science, Office of Advanced Scientific Computing Research, Scientific Discovery through Advanced Computing (SciDAC) program under the contract No. DE-AC02-05CH11231. This research used resources of the National Energy Research Scientific Computing Center, a DOE Office of Science User Facility supported by the Office of Science of the U.S. Department of Energy under Contract No. DE-AC02-05CH11231 using NERSC award ASCR-ERCAP-m1027.

Appendix A Proof of Theorem 3.1

According to Theorem 2.1, any smooth curve $\gamma(s) \in \mathcal{M}_r$ can be written as a tensor cross interpolant with nested indices

$$\gamma(s) = \prod_{k=1}^d \gamma(\mathcal{I}^{\leq k-1}, :, \mathcal{I}^{>k}; s) [\gamma(\mathcal{I}^{\leq k}, \mathcal{I}^{>k}; s)]^{-1}. \quad (64)$$

Thus any tangent vector $\delta \mathbf{f} \in T_{\mathbf{f}} \mathcal{M}_r$ is given by

$$\delta \mathbf{f} = \frac{d}{ds} \left[\prod_{k=1}^d \gamma(\mathcal{I}^{\leq k-1}, :, \mathcal{I}^{>k}; s) [\gamma(\mathcal{I}^{\leq k}, \mathcal{I}^{>k}; s)]^{-1} \right]_{s=0}. \quad (65)$$

Because the indices are nested (27), we have the interpolation property (28) from which we obtain

$$\delta \mathbf{f}(\mathcal{I}^{\leq k-1}, :, \mathcal{I}^{>k}) = \frac{d}{ds} \gamma(\mathcal{I}^{\leq k-1}, :, \mathcal{I}^{>k}; s)|_{s=0}. \quad (66)$$

Setting

$$\frac{d}{ds} \gamma(\mathcal{I}^{\leq k-1}, :, \mathcal{I}^{>k}; s)|_{s=0} = \mathbf{X}(\mathcal{I}^{\leq k-1}, :, \mathcal{I}^{>k}), \quad (67)$$

shows the existence of the tangent vector. Expanding (65) using the product rule we can write the tangent vector as

$$\begin{aligned} \delta \mathbf{f} &= \sum_{p=1}^d \prod_{k=1}^{p-1} \mathbf{f}(\mathcal{I}^{\leq k-1}, :, \mathcal{I}^{>k}) [\mathbf{f}(\mathcal{I}^{\leq k}, \mathcal{I}^{>k})]^{-1} \\ &\times \left(\mathbf{X}(\mathcal{I}^{\leq k-1}, :, \mathcal{I}^{>k}) [\mathbf{f}(\mathcal{I}^{\leq k}, \mathcal{I}^{>k})]^{-1} \right. \\ &\quad \left. - \mathbf{f}(\mathcal{I}^{\leq k-1}, :, \mathcal{I}^{>k}) [\mathbf{f}(\mathcal{I}^{\leq k}, \mathcal{I}^{>k})]^{-1} \mathbf{X}(\mathcal{I}^{\leq k}, \mathcal{I}^{>k}) [\mathbf{f}(\mathcal{I}^{\leq k}, \mathcal{I}^{>k})]^{-1} \right) \\ &\times \prod_{k=p+1}^d \mathbf{f}(\mathcal{I}^{\leq k-1}, :, \mathcal{I}^{>k}) [\mathbf{f}(\mathcal{I}^{\leq k}, \mathcal{I}^{>k})]^{-1}. \end{aligned} \quad (68)$$

Now suppose $\widehat{\delta \mathbf{f}} \in T_{\mathbf{f}} \mathcal{M}_r$ is another tangent vector satisfying

$$\widehat{\delta \mathbf{f}}(\mathcal{I}^{\leq k-1}, :, \mathcal{I}^{>k}) = \mathbf{X}(\mathcal{I}^{\leq k-1}, :, \mathcal{I}^{>k}).$$

Since $\widehat{\delta \mathbf{f}} \in T_{\mathbf{f}} \mathcal{M}_r$, there exists a curve $\widehat{\gamma}(s)$ on \mathcal{M}_r passing through \mathbf{f} at $s = 0$ such that

$$\widehat{\delta \mathbf{f}} = \frac{d}{ds} \widehat{\gamma}(s)|_{s=0}. \quad (69)$$

According to Theorem 2.1, the curve $\widehat{\gamma}(s)$ can also be written as a tensor cross interpolant

$$\widehat{\gamma}(s) = \prod_{k=1}^d \widehat{\gamma}(\mathcal{I}^{\leq k-1}, :, \mathcal{I}^{>k}; s) [\widehat{\gamma}(\mathcal{I}^{\leq k}, \mathcal{I}^{>k}; s)]^{-1}, \quad (70)$$

which implies that

$$\begin{aligned} \frac{d}{ds} \widehat{\gamma}(\mathcal{I}^{\leq k-1}, :, \mathcal{I}^{>k}; s)|_{s=0} &= \widehat{\delta \mathbf{f}}(\mathcal{I}^{\leq k-1}, :, \mathcal{I}^{>k}) \\ &= \mathbf{X}(\mathcal{I}^{\leq k-1}, :, \mathcal{I}^{>k}). \end{aligned} \quad (71)$$

Expanding (69) using the product rule we find that $\widehat{\delta \mathbf{f}}$ is equal to $\delta \mathbf{f}$ in (68).

References

- [1] S. M. Allen and J. W. Cahn. Ground state structures in ordered binary alloys with second neighbor interactions. *Acta Metallurgica*, 20(3):423–433, 1972.
- [2] C. Cercignani. *The Boltzmann equation and its applications*. Springer, 1988.
- [3] G. Ceruti and C. Lubich. An unconventional robust integrator for dynamical low-rank approximation. *BIT Numerical Mathematics*, 62(1):23–44, Mar 2022.
- [4] G. Ceruti, C. Lubich, and H. Walach. Time integration of tree tensor networks. *SIAM J. Num. Anal.*, 59(1):289–313, 2021.
- [5] S. Chaturantabut and D. C. Sorensen. Nonlinear model reduction via discrete empirical interpolation. *SIAM Journal on Scientific Computing*, 32(5):2737–2764, 2010.
- [6] H. A. Daas, G. Ballard, P. Cazeaux, E. Hallman, A. Miedlar, M. Pasha, T. W. Reid, and A. K. Saibaba. Randomized algorithms for rounding in the tensor-train format. *SIAM Journal on Scientific Computing*, 45(1):A74–A95, 2023.
- [7] A. Dektor, A. Rodgers, and D. Venturi. Rank-adaptive tensor methods for high-dimensional nonlinear PDEs. *J. Sci. Comput.*, 88(36):1–27, 2021.
- [8] A. Dektor and D. Venturi. Dynamically orthogonal tensor methods for high-dimensional nonlinear PDEs. *J. Comput. Phys.*, 404:109125, 2020.
- [9] A. Dektor and D. Venturi. Dynamic tensor approximation of high-dimensional nonlinear PDEs. *J. Comput. Phys.*, 437:110295, 2021.
- [10] A. Dektor and D. Venturi. Tensor rank reduction via coordinate flows. *J. Comput. Phys.*, 491:112378, 2023.
- [11] A. Dektor and D. Venturi. Coordinate-adaptive integration of pdes on tensor manifolds. *Communications on Applied Mathematics and Computation*, 2024.
- [12] S. Dolgov and D. Savostyanov. Parallel cross interpolation for high-precision calculation of high-dimensional integrals. *Computer Physics Communications*, 246:106869, 2020.
- [13] M. Donello, G. Palkar, M. H. Naderi, D. C. Del Rey Fernández, and H. Babae. Oblique projection for scalable rank-adaptive reduced-order modelling of nonlinear stochastic partial differential equations with time-dependent bases. *Proceedings of the Royal Society A: Mathematical, Physical and Engineering Sciences*, 479(2278):20230320, 2023.
- [14] W. Gangbo, W. Li, S. Osher, and M. Puthawala. Unnormalized optimal transport. *J. Comput. Phys.*, 399:108940, 2019.
- [15] B. Ghahremani and H. Babae. A DEIM Tucker tensor cross algorithm and its application to dynamical low-rank approximation. *arXiv:2401.04249*, pages 1–23, 2024.
- [16] J. S. Hesthaven, S. Gottlieb, and D. Gottlieb. *Spectral methods for time-dependent problems*, volume 21 of *Cambridge Monographs on Applied and Computational Mathematics*. Cambridge University Press, Cambridge, 2007.
- [17] S. Holtz, T. Rohwedder, and R. Schneider. On manifolds of tensors of fixed TT-rank. *Numer. Math.*, 120(4):701–731, 2012.
- [18] A.-K. Kassam and L. N. Trefethen. Fourth-order time-stepping for stiff PDEs. *SIAM Journal on Scientific Computing*, 26(4):1214–1233, 2005.
- [19] E. Kieri and B. Vandereycken. Projection methods for dynamical low-rank approximation of high-dimensional problems. *Comput. Methods Appl. Math.*, 19(1):73–92, 2019.

- [20] D. Kressner and C. Tobler. Algorithm 941: Htucker—a matlab toolbox for tensors in hierarchical tucker format. 40(3), 2014.
- [21] C. Lubich, I. V. Oseledets, and B. Vandereycken. Time integration of tensor trains. *SIAM J. Numer. Anal.*, 53(2):917–941, 2015.
- [22] M. H. Naderi and H. Babae. Adaptive sparse interpolation for accelerating nonlinear stochastic reduced-order modeling with time-dependent bases. *Computer Methods in Applied Mechanics and Engineering*, 405:115813, 2023.
- [23] I. Oseledets and E. Tyrtyshnikov. TT-cross approximation for multidimensional arrays. *Linear Algebra and its Applications*, 432(1):70–88, 2010.
- [24] I. V. Oseledets. Tensor-train decomposition. *SIAM J. Sci. Comput.*, 33(5):2295—2317, 2011.
- [25] B. Peherstorfer, Z. Drmač, and S. Gugercin. Stability of discrete empirical interpolation and gappy proper orthogonal decomposition with randomized and deterministic sampling points. *SIAM Journal on Scientific Computing*, 42(5):A2837–A2864, 2020.
- [26] Z. Qin, A. Lidiak, Z. Gong, G. Tang, M. B. Wakin, and Z. Zhu. Error analysis of tensor-train cross approximation. *Advances in Neural Information Processing Systems*, 35:14236–14249, 2022.
- [27] H. Risken. *The Fokker-Planck equation: methods of solution and applications*. Springer-Verlag, second edition, 1989. Mathematics in science and engineering, vol. 60.
- [28] A. Rodgers, A. Dektor, and D. Venturi. Adaptive integration of nonlinear evolution equations on tensor manifolds. *J. Sci. Comput.*, 92(39):1–31, 2022.
- [29] D. Savostyanov. Quasioptimality of maximum-volume cross interpolation of tensors. *Linear Algebra Appl.*, 458:217–244, 2014.
- [30] D. C. Sorensen and M. Embree. A DEIM induced CUR factorization. *SIAM Journal on Scientific Computing*, 38(3):A1454–A1482, 2016.
- [31] A. Uschmajew and B. Vandereycken. The geometry of algorithms using hierarchical tensors. *Linear Algebra Appl.*, 439(1):133–166, 2013.
- [32] D. Venturi. The numerical approximation of nonlinear functionals and functional differential equations. *Physics Reports*, 732:1–102, 2018.
- [33] D. Venturi and A. Dektor. Spectral methods for nonlinear functionals and functional differential equations. *Res. Math. Sci.*, 8(27):1–39, 2021.